Observations and Analysis of Organic Aerosol Evolution in Some Prescribed Fire Smoke Plumes

A.A. May[1,2]*, T. Lee[1,3], G.R. McMeeking[1,4], S. Akagi[5], A.P. Sullivan[1], S. Urbanski[6], R.J. Yokelson[5], S.M. Kreidenweis[1]*

1 Department of Atmospheric Science, Colorado State University, Fort Collins, CO, USA

2 Now with Department of Civil, Environmental and Geodetic Engineering, The Ohio State University, Columbus, OH, USA

3 Now with Department of Environmental Science, Hankuk University of Foreign Studies, Yongin, Korea

4 Now with Droplet Measurement Technologies, Boulder, CO, USA

5 Department of Chemistry, University of Montana, Missoula, MT, USA

6 Missoula Fire Sciences Laboratory, Rocky Mountain Research Station, US Forest Service, Missoula, MT, USA

* Corresponding authors: A.A. May, may.561@osu.edu; S.M. Kreidenweis, sonia@atmos.colostate.edu

Abstract

Open biomass burning is a significant source of primary air pollutants such as particulate matter (PM) and non-methane organic gases (NMOG). However, the physical and chemical atmospheric processing of these emissions during transport is poorly understood. Atmospheric transformations of biomass burning emissions have been investigated in environmental chambers, but there have been limited opportunities to investigate these transformations in the atmosphere. In this study, we deployed a suite of real-time instrumentation on a Twin Otter aircraft to sample smoke from prescribed fires in South Carolina, conducting measurements at both the source and downwind to characterize smoke evolution with atmospheric aging. Organic aerosol (OA) within the smoke plumes was quantified using an Aerosol Mass Spectrometer (AMS), along with refractory black carbon (rBC) using a Single Particle Soot Photometer and carbon monoxide (CO) and carbon dioxide (CO_2) using a Cavity Ring-Down Spectrometer. During the two fires for which we were able to obtain aerosol aging data, normalized excess mixing ratios and "export factors" of conserved species (rBC, CO, CO_2) suggested that changes in emissions at the source did not account for most of the differences observed in samples of increasing age. Investigation of AMS mass fragments indicated that the in-plume fractional contribution ($f_{m/z}$) to OA of the primary fragment (m/z 60) decreased downwind, while the fractional contribution of the secondary fragment (m/z 44) increased. Increases in f_{44} are typically interpreted as indicating chemical aging of OA. Likewise, we observed an increase in the O:C elemental ratio downwind, which is usually associated with aerosol aging. However, the rapid mixing of these plumes into the background air suggests that these chemical transformations may be attributable to the different volatilities of the compounds that fragment to these m/z in the AMS. The gas-particle partitioning behavior of the bulk OA observed during the study was

consistent with the predictions from a parameterization developed for open biomass burning emissions in the laboratory. Furthermore, we observed no statistically-significant increase in total organic mass with atmospheric transport. Hence, our results suggest that dilution-driven evaporation likely dominated over chemical production of SOA within our smoke plumes, likely due to the fast dilution and limited aging times (< ~5 hr) that we could sample.

1. Introduction

Open biomass burning is estimated to be the largest contributor on a global scale to atmospheric fine carbonaceous particulate matter (PM) (Bond et al., 2013) and the second largest contributor to atmospheric non-methane organic gases (NMOG) (Akagi et al., 2011). Substantial research has been focused on characterizing gas- and particle-phase primary emissions from biomass burning and the development of emission inventories (Akagi et al., 2011; Burling et al., 2010, 2011; Christian et al., 2003; Hosseini et al., 2013; May et al., 2014; McMeeking et al., 2009; Reid et al., 2005; Urbanski, 2013; Urbanski et al., 2011; Watson et al., 2011; van der Werf et al., 2010; Wiedinmyer et al., 2006, 2011; Yokelson et al., 2013a). These emissions are ultimately integrated into chemical transport models used to predict regional air quality and global climate impacts.

Organic aerosol (OA) species represent the major component by mass in the submicron carbonaceous PM emitted from fires (May et al., 2014; McMeeking et al., 2009; Reid et al., 2005). In general, the physical and chemical evolution of biomass-burning-derived OA in the atmosphere after emission is poorly understood, in part because OA is a "metastable intermediate" (Donahue et al., 2013). Since OA consists of thousands of species with a spectrum of temperature-dependent saturation vapor pressures, the portion of OA that is observable as PM varies with dilution and with atmospheric temperature. Further, many of the species comprising

OA have been shown to undergo oxidation reactions, forming secondary products with their own range of volatilities. In field studies, OA in biomass burning plumes has been observed to be enhanced, be depleted, or remain constant with time after emission (Akagi et al., 2012; Capes et al., 2008; Cubison et al., 2011; DeCarlo et al., 2008; Jolleys et al., 2012; Vakkari et al., 2014; Yokelson et al., 2009), but due to the complexities described above, attribution of these transformations to specific physical and chemical processes is difficult (Heilman et al., 2014).

Laboratory studies have been conducted to attempt to separate these processes for biomass-burning-derived OA. As part of the third Fire Lab at Missoula Experiment (FLAME-III), May et al. (2013) derived a volatility distribution and related thermodynamic parameters representative of the primary emissions from all of the biomass fuels studied. In that same study, Hennigan et al. (2011) and Ortega et al. (2013) investigated chemical transformations of the emissions using an environmental chamber and a potential aerosol mass chamber, respectively. Results from both chambers demonstrated that the OA mass can be enhanced, depleted, or remain roughly constant with oxidation, similar to field measurements, yet the OA always became apparently more oxidized with photochemical aging, as interpreted from the organic mass fragments measured via online aerosol mass spectrometry.

In this work, we report and interpret observations from the South Carolina fiRe Emissions And Measurements (SCREAM) campaign conducted in October-November 2011 (Akagi et al., 2013, 2014; May et al., 2014; Sullivan et al., 2014). The objectives of SCREAM were to: (1) simulate moderately intense wildfires by conducting prescribed burns at sites with high fuel loadings, (2) characterize the emissions and develop estimates of emission factors and emission ratios from both ground- and aircraft-based sampling, and (3) sample plumes downwind as they evolved during atmospheric transport. We also sampled fires of opportunity

during the study. The SCREAM campaign combined simultaneous aircraft-based online measurements of refractory black carbon (rBC), time-resolved non-refractory sub-micron PM measurements (including OA), and time-resolved water-soluble organic carbon (WSOC) and levoglucosan (LEV) measurements in addition to a suite of gas-phase compounds. Companion papers have reported airborne trace gas emissions (Akagi et al., 2013), ground-based trace gas emissions (Akagi et al., 2014), airborne WSOC and smoke marker emissions (Sullivan et al., 2014), and airborne primary PM emissions (May et al., 2014). This paper focuses on airborne observations of the OA mass concentrations and composition near the source and transformations to OA mass concentration and composition during the first hours of atmospheric transport.

2. Methods

Emissions from five of the seven fires sampled during SCREAM are discussed in this paper. Details including fuel type, area burned, meteorology and stand history were provided by Akagi et al. (2013) and are summarized briefly here. Two of the burns were conducted on the Fort Jackson (FJ) Army Base (located northeast of Columbia, SC) in Blocks 9b (FJ 9b; 34º0'15" N, 80º52'37" W; 1 November 2011) and 22b (FJ 22b; 34º5'4" N, 80º52'16" W; 2 November 2011). These burns occurred in older stands that had not been treated for a number of years, and were intended to simulate wildfires. Fuel inventories indicated that the vegetation comprised primarily of mature longleaf pine (*Pinus palustris*) and loblolly pine (*Pinus taeda*) with some contributions of turkey oak (*Quercus laevis Walter*) and farkleberry (*Vaccinium arboretum Marsh.*). Complementary ground-based measurements of emissions from the FJ burns were reported by Akagi et al. (2014). The three other sampled fires were designated Georgetown (33º12'9" N,

79º24’6” W; 7 November 2011), Francis Marion (33º12’55” N, 79º28’34” W; 8 November 2011), and Bamberg (33º14’5” N, 80º56’41” W; 10 November 2011), based on the location in SC where the fire occurred. Georgetown and Francis Marion were located in coastal SC, likely burning coastal grasses and longleaf pine understory, respectively, based on in-flight observations. The Bamberg fire, located roughly 80 km due south of the Fort Jackson site in inland SC, was likely comprised of multiple fuel types, including longleaf/loblolly pine understory as well as marsh grasses, based on smoke marker ratio measurements reported in Sullivan et al. (2014).

2.1. Sample Collection

Smoke plumes during SCREAM were sampled via airborne measurements onboard a United States Forest Service DHC-6 Twin Otter aircraft. Sampling strategies and flight tracks are described in prior literature from the SCREAM study (Akagi et al., 2013; May et al., 2014; Sullivan et al., 2014). Fires were initiated in mid-morning, and the aircraft initially sampled the emissions near the source. Following the source characterization period, the downwind plume was sampled to investigate the effect of chemical and physical aging during atmospheric transport. For consistency with May et al. (2014), we defined “near-source” samples as those collected within 5 km of the fire (always less than 30 minutes of aging, but most of the smoke had an age of < 10 minutes based on average ambient wind speed), while downwind samples were those collected at distances greater than 5 km. During flights, there were also periods of out-of-plume background sampling to establish time-dependent background concentrations of the species that were quantified in the plume.

The flight path for the FJ 9b burn is provided in Figure 1 as one example. Figure 1a provides total (i.e., not background-corrected) OA mass concentration (C_{OA}), which was typically between 3-7 μg m^{-3} (average = 4.6 μg m^{-3}) outside of the plume throughout the

sampling domain, with the exception of higher concentrations attributable to the smoke plume. Correcting the data for the background OA results in Figure 1b; here, the plume transport is more distinct.

The first 1-2 hours of flight time was typically spent sampling near the source at ~100-600 m altitude. Following this characterization period, it was possible to sample smoke downwind with 1-2 hours of atmospheric aging, so we then alternated downwind cross-plume samples with occasional additional source sampling. A challenge was that emissions were rapidly diluted and mixed within the boundary layer, and the plumes did not penetrate into the free troposphere, so visual tracking of the plumes was challenging. In fact, the flight path was guided via consultation with real-time instrument output, which enabled the identification of plume center and extent as well as the marking of way points. Furthermore, the plume from the FJ 22b fire entered restricted air space near Columbia, SC, so it was only possible to follow this plume for a short distance from the point of emission.

Downwind, the Twin Otter typically flew at altitudes between 500 m and 1500 m, but not with sufficient detail to develop vertical profiles. All data, regardless of sampling altitude (or latitude/longitude), are categorized as "within the plume" or "outside of the plume" along with the additional distinction of "estimated time since emission" (please refer to Section 2.3.1).

2.2. Instrumentation

The instrumentation installed on the Twin Otter used to characterize emissions included a High-Resolution Time-of-Flight Aerosol Mass Spectrometer (HR-ToF-AMS; Aerodyne Research, Inc.), a Single Particle Soot Photometer (SP2; Droplet Measurement Technologies, Inc.), a Cavity Ring-Down Spectrometer (CRDS; Picarro G2401; Picarro, Inc.), an airborne Fourier-transform infrared spectrometer (AFTIR), a Particle-into-Liquid Sampler/Total Organic Carbon and fraction collector system (Sullivan et al., 2014) and an Aircraft Integrated

Meteorological Measuring System (AIMMS-20) probe (Aventech Research, Inc.). The AIMMS-20 provided meteorological data such as three-dimensional wind vectors, three-dimensional position of the aircraft (i.e., latitude, longitude, and altitude), ambient temperature, and ambient relative humidity. All sampling was conducted from a low turbulence inlet (Wilson et al., 2004) followed by a non-rotating Micro Orifice Uniform Deposit Impactor (MOUDI; Marple et al., 1991). The MOUDI was operated such that it served as a PM_1 selector (i.e., having 50% particle transmission efficiency for particulate matter of 1 μm aerodynamic diameter with a sharpness of 1.08 – particles less than roughly 900 nm will be transmitted with 100% efficiency). All data were adjusted to the same timestamp via alignment of peaks (thus accounting for differences in both instrument clocks and instrument response times), which we referenced to the HR-ToF-AMS.

2.2.1. Aerosol Mass Spectrometer

The HR-ToF-AMS (hereafter AMS) characterizes non-refractory sub-micron aerosol by focusing sampled particles through an aerodynamic lens, collecting particles on a thermal vaporizer, ionizing the vaporized particles via electron impaction, and detecting ions (m/z) in the high-resolution time-of-flight mass spectrometer (DeCarlo et al., 2006). Using the ToF-AMS data analysis toolkit SQUIRREL/PIKA (Sueper et al., 2013), aerosol mass concentrations can be reconstructed from the m/z signal; for this study, we fit HR peaks for $m/z \leq 200$. These concentrations are dependent on instrument parameters (e.g., ionization efficiency and vaporizer collection efficiency). Ionization efficiency calibrations were performed with 350 nm ammonium nitrate particles throughout the campaign, with values ranging from 1.83×10^{-7} to 2.91×10^{-7} ions molecule^{-1}. Composition-dependent collection efficiencies were calculated following the algorithm of Middlebrook et al. (2012), which is now built into the SQUIRREL software, for each AMS sample and ranged from roughly 0.5-0.9, with a campaign-average value of 0.53. We

report AMS-derived emissions data of nitrate, sulfate, ammonium, and chloride elsewhere (May et al., 2014). As stated in May et al. (2014), our results are potentially biased by up to a factor of two due to the inherent uncertainty in our estimation of CE.

The AMS was mounted into National Center for Atmospheric Research GV-type aircraft racks with a pressure-controlled inlet to reduce fluctuations of the pressure within the aerodynamic lens (Bahreini et al., 2008). During operation, data were exclusively collected using the "V-mode" of the ion time-of-flight within the mass spectrometer; since no particle time-of-flight data were collected, no size-resolved information is available. AMS data were typically collected with a time resolution of 6 seconds (corresponding to a distance of roughly 250-300 m).

While we obtained simultaneous measurements of gas-phase CO_2, we utilized the standard correction in the fragmentation table from Allan et al. (2004), rather than explicit corrections for CO_2 to account for differences within and without the plume. The AMS samples particles roughly 10^7 times more efficiently than the gas-phase. We estimate that on average, our plume OA concentrations are positively biased by 0.0044 ± 0.0019% (both near the source and downwind), our background OA concentrations are positively biased by 0.025 ± 0.021%, and our *m*/*z* 44 measurements are positively biased by 0.20 ± 0.11%, all based on co-located gas-phase CO_2 measurements. Consequently, we deemed this correction unnecessary as this interference represents < 0.5% of our reported values.

2.2.2. Single Particle Soot Photometer

The SP2 provides operationally-defined rBC mass concentrations via laser-induced incandescence (Stephens et al., 2003; Schwarz et al., 2006). Absorbing material present in particles is heated to its vaporization temperature and emits radiation, which is measured by optical detectors. This approach removes uncertainties due to interferences of artifacts that have

been observed during filter-based approaches (Kirchstetter et al., 2004) and excludes the influence of "brown" carbon that can bias optical absorption methods (Andreae and Gelencsér, 2006; Lack et al., 2012), although it has been shown the method responds to some metals. Signal is related to rBC mass via calibration procedures; during SCREAM, calibrations were performed using fullerene soot. Generally, rBC mass concentrations were recorded every 6 seconds, similar to the AMS. Additional details related to the SP2 operation during this campaign can be found in May et al. (2014).

2.2.3. Cavity Ring-Down Spectrometer

A Picarro G2401 provided 0.5 Hz measurements of CO_2, CO, CH_4, and H_2O, which are the major gas-phase emissions from combustion sources. The CRDS was calibrated in-flight using mixed standards of CO_2/CO/CH_4 and procedures similar to those described by Urbanski (2013). These data were applied to calculate emission ratios and emission factors of particle-phase species, as described below.

2.3. Data Processing

2.3.1 Plume Identification and Age

As discussed previously, visual plume identification was challenging. Positive downwind plume intercepts were confirmed through simultaneous spikes in measured values of OA, BC, and CO. These confirmed intercepts were corroborated by simultaneous increases in smoke markers (Sullivan et al., 2014) and trace gases (Akagi et al., 2013). Intercept-averaged concentrations for each transect were derived by integrating the excess area (above background) under the data time series curves and dividing by the elapsed time in the window of integration.

Sample ages (times since emission) were estimated using the distance from the source and mean wind speed. Distance from the source was computed using the haversine formula and the spatial coordinates measured by the AIMMS-20. Mean wind speed was also measured using

229 the AIMMS-20. Akagi et al. (2013) estimated that this approach has an uncertainty of roughly
230 30%, largely due to uncertainties in the wind speed data. Due to the plume tracking challenges,
231 plume intercepts were rarely perfectly perpendicular to the plume and were often diagonal
232 transects. Thus, a given sample can be associated with a range of estimated ages. In subsequent
233 figures, we plot the average age of a plume intercept along with error bars representing the range
234 of ages; in these figures, we do not include the estimated uncertainty of 30% on this range.
235
236 In-plume data from all research flights were corrected for local background
237 concentrations via integration under the curves in data time series between out-of-plume
238 measurements. The resulting species concentrations are "excess" concentrations and denoted by
239 the delta symbol, i.e., ΔX is the excess concentration of species X. We show background values
240 of some parameters in some of the following figures; these background concentrations represent
241 the median background concentration for the duration of the given flight. Sample background-
242 corrected data are provided in Figure 1.

243 2.3.2. Excess Emission Ratios and Emission Factors

244 Normalized excess mixing ratios (NEMR) are often used to account for transient fire
245 behavior and the dilution and mixing of plumes with background air during transport (e.g.,
246 Hobbs et al., 2003) and are defined as:

247 $$NEMR_X = \frac{\Delta X}{\Delta CO} \qquad (1)$$

248 where ΔX is the excess concentration of species X, and ΔCO is the background-corrected value
249 of CO. Since both numerator and denominator are excess quantities, uncertainties in their values
250 increase as the plume dilutes and in-plume concentrations approach the background
251 concentrations. Here, we report plume-integrated $NEMR_X$ for each plume interception, so our

values differ from the "fire-integrated" values (based on consideration of all the plume intercepts) reported in May et al. (May et al., 2014). $NEMR_X$ are reported here in units of μg m^{-3} ppmv-CO^{-1}; this value can be converted to g g-CO^{-1} by multiplying by a factor of 8.7 x 10^{-4} ppmv-CO (μg-CO m^{-3})$^{-1}$. Strictly speaking, $NEMR_X$ is a misnomer for aerosol mass concentrations, but we utilize this terminology for consistency with the vast body of prior literature.

Time series of instantaneous $NEMR_X$ provide information on transient smoke behavior (Jolleys et al., 2014). By associating instantaneous $NEMR_X$ with time since emission, physicochemical transformations can be investigated, since $NEMR_X$ accounts for dilution and thus should be constant with time in the absence of sources or sinks of the species X or changes in the initial emissions. The net formation of secondary organic aerosol (SOA) in smoke plumes can be inferred from an increase in $NEMR_{OA}$ with distance downwind (Yokelson et al., 2009). On the other hand, since OA emitted from biomass burning sources is semi-volatile, net evaporation of particle-phase mass as dilution proceeds would appear as a decrease in $NEMR_{OA}$ (Akagi et al., 2012).

Emission factors (EF) are widely used descriptors of fire emissions (Ward and Radke, 1993; Andreae and Merlet, 2001). Their calculation relates the mass of X emitted (M_X) to the mass of dry fuel consumed (M_{fuel}). In cases where the mass of fuel consumed is unknown, a carbon mass balance approach can be applied, which relates the change in the concentration of X relative to the background (ΔX; μg m^{-3}) to the excess carbon concentrations (i.e., background-corrected concentrations that have been converted to mg-C m^{-3}) of CO_2, CO, total organic gases (TOG = CH_4 + NMOG), and carbonaceous PM (PM_C):

$$EF_X = \frac{M_X}{M_{fuel}} = \frac{\Delta X}{\Delta CO_2 + \Delta CO + \Delta TOG + \Delta PM_c} f_C \qquad (2)$$

In Equation 2, the term f_C is a conversion factor representing fuel carbon content. Since we lack detailed fuel information, we assume that $f_C = 0.50$, roughly the average fuel carbon content of southeastern (SE) US coastal plain biomass fuels reported in laboratory studies (Burling et al., 2010; May et al., 2014; McMeeking et al., 2009). Since ΔTOG and $\Delta PM_C << (\Delta CO_2 + \Delta CO)$, for convenience we approximate EF_X neglecting both ΔTOG and ΔPM_C, which results in an over-estimate in EF_X of ~3-5% (Yokelson et al., 2013b). Like $NEMR_X$, EF_x are based on excess concentrations and account for dilution, but if an "emission factor" is computed with downwind data, the value obtained reflects changes in the initial emission factor plus the effect of any sources or sinks of the originally-emitted species X. Hereafter, we will refer to downwind "emission factors" as "export factors", also denoted as EF_X and calculated from Equation 2; the main distinction is that an export factor describes X downwind from the source, and thus may be subject to both changes in the emissions as the fire burns and atmospheric transformations. We report EF_X as g or mg kg-dry-fuel^{-1}.

3. Results and Discussion

During the study, only two fires provided adequate downwind aerosol data allowing us to investigate in-plume aerosol physicochemical transformations: the FJ 9b fire and the Francis Marion fire. As mentioned earlier, the plume from the FJ 22b fire entered restricted airspace and could not be pursued. Further, the Georgetown fire was a small fire whose plume rapidly mixed with the background, so downwind ΔOA was small and uncertain; the Bamberg samples represented two distinct fuel types as shown elsewhere (May et al., 2014; Sullivan et al., 2014), making it difficult to distinguish transformations during transport from differences in the sources.

297 In Figure 2, we present composition data versus estimated time since emission for the
298 NEMR or EF for four major components present in the biomass burning smoke sampled for the
299 FJ 9b fire: OA ($NEMR_{OA}$; Figure 2a), rBC ($NEMR_{rBC}$; Figure 2b), CO (EF_{CO}; Figure 2c), and
300 CO_2 (EF_{CO2}; Figure 2d). Data near the source are presented as box-and-whisker plots (25^{th}-75^{th}
301 and 10^{th}-90^{th} percentiles); these data were collected during roughly 2.5 hours of sampling during
302 which the modified combustion efficiency (MCE) (Ward and Radke, 1993) varied between 0.900
303 and 0.930, which explains some of the variability in the data. Data up to five hours downwind
304 were obtained and are shown as open symbols. For downwind samples, vertical errors bars
305 represent estimated measurement uncertainties while horizontal error bars represent the range of
306 estimated plume ages for non-perpendicular plume transects; horizontal error bars do not account
307 for the estimated 30% measurement uncertainty in wind speed. To assess whether differences
308 near the source and downwind are statistically significant, we conducted unpaired *t*-tests. When
309 the corresponding two-tailed *p* value ≤ 0.05, we consider the results to be significantly different;
310 conversely, if the *p* value > 0.05, we infer that there is no significant difference.
311 We expect rBC, CO, and CO_2 to be conserved with transport since they are stable in the
312 atmosphere on the timescales considered here. Indeed, unpaired *t*-tests for the data shown in
313 Figures 2b-d indicate that there was no significant difference in the average value of these
314 species at the source and downwind (two-tailed *p* values > 0.13). Differences in mean downwind
315 EFs are attributable to measurement uncertainties, including identification of the plume edges,
316 and variability in the combustion at the source. Fitting an exponential decay with distance from
317 the source of absolute mixing ratios of CO and CO_2, we infer an average mixing rate (the inverse
318 of the dilution timescale, or the time to decay by 1/e) of 1.6 hr^{-1} during the FJ 9b experiment.

Since OA is reactive and semi-volatile, it is perhaps not surprising that the downwind $NEMR_{OA}$ over 2-5 hr of atmospheric aging is significantly lower than the $NEMR_{OA}$ at the source (Figure 2a; two-tailed *p* value = 0.015), suggesting a net loss of emitted OA via evaporation and/or reaction. As demonstrated by Akagi et al. (2013), the smoke plume was photochemically active, as evident through enhancements of ozone and formaldehyde relative to the source.

Figure 3 is identical to Figure 2 but represents the Francis Marion burn, the only other case with downwind aerosol measurements adequate to assess aging (here, up to 1.5 hr after emission). Akagi et al. (2013) inferred photochemical processing was occurring in the Francis Marion plume, based on observed downwind enhancements of ozone and formaldehyde relative to the source. However, unlike the FJ 9b fire, none of the computed downwind NEMR and EF shown in Fig. 3 were significantly different from the source (all two-tailed *p* values > 0.32). The background OA concentrations, which we assume contribute to gas-particle partitioning of emitted OA by providing additional absorptive material, were roughly 50% greater during the Francis Marion fire compared to the FJ 9b fire; furthermore, the mixing rate was 20% slower for the Francis Marion plume (1.3 hr^{-1}), and the plume aging was observed over a much shorter time period. These factors would slow the evaporation of emitted OA, and limit the time over which chemical transformations could occur and be observed. Indeed, over the first 1.5 hr after emission, the data for FJ 9b shown in Figure 2 also indicated no statistically-significant change in $NEMR_{OA}$.

3.1. Chemical Transformations of Organic Aerosol

In this section, we investigate chemical transformations of the organic aerosol, fragment evolution (Figure 4), and elemental ratio analyses (Figure 5) using two approaches to for both fires with adequate downwind data: the FJ 9b and Francis Marion burns. Both Ng et al. (2010)

342 and Morgan et al. (2010) demonstrated that "fresh" OA in ambient samples can be distinguished
343 by organic fragment signatures in the mass spectra (e.g., $C_3H_7^+$ at *m*/*z* 43), while "aged" OA is
344 more highly oxidized and can be distinguished by a strong contribution of CO_2^+ (*m*/*z* 44). The
345 fractional contributions of each of these fragments to the total OA concentration (e.g., f_{44} =
346 C_{44}/C_{OA}, where C_{44} is the mass concentration of particulate CO_2^+, which is likely due to
347 decarboxylation on the vaporizer surface rather than CO_2 molecules being present in the aerosol
348 sample) change with atmospheric aging: f_{43} is expected to decrease and f_{44} to increase.

349 However, neither Ng et al. (2010) nor Morgan et al. (2010) directly considered the
350 influence of biomass burning. Cubison et al. (2011) and Ortega et al. (2013) thus modified the
351 approach and compared f_{60} and f_{44} to infer photochemical aging of BBOA. Levoglucosan and
352 other anhydrosugars are pyrolysis products of cellulose, and thus are used as molecular markers
353 for biomass burning emissions (Simoneit et al., 1999; Sullivan et al., 2008); these compounds
354 contribute to AMS spectra at *m*/*z* 60 ($C_2H_4O_2^+$) (Alfarra et al., 2007; Lee et al., 2010). May et al.
355 (2012) and references therein demonstrated that levoglucosan is semi-volatile at ambient
356 conditions and thus *m*/*z* 60 could decrease due to evaporation during dilution, if this finding is
357 extrapolated to all contributing species. Furthermore, Hennigan et al. (2010) demonstrated that
358 levoglucosan is reactive and chemically decays similar to the hydrocarbon-like (*m*/*z* 43)
359 fragments. Thus, f_{60} may change due to both dilution-driven evaporation and photo-oxidation
360 processes.

361 In Figure 4, we present excess f_{60} (Δf_{60}) and excess f_{44} (Δf_{44}) for the FJ 9b and Francis
362 Marion fires. These excess fragment fractional contributions were computed from background-
363 corrected *m*/*z* 60 or *m*/*z* 44 mass concentrations by dividing that excess concentration by ΔOA.
364 Thus, as the plume dilutes and becomes less distinguishable from the background, Δf_{60} and Δf_{44}

should remain constant if neither preferentially evaporates, reacts, or accumulates within the plume. For the FJ 9b fire, the source-downwind differences for both Δf_{60} (Figure 4a) and Δf_{44} (Figure 4b) are statistically significant (two-tailed p value < 0.0001). For the Francis Marion fire, Δf_{60} (Figure 4c) is significantly lower downwind than at the source (two-tailed p value < 0.0001), while Δf_{44} (Figure 4d) is significantly higher downwind than at the source (two-tailed p value = 0.029). The result for Δf_{60} is consistent with Figure 2a; that is, the decrease in Δf_{60} downwind during the FJ 9b fire reflects the decrease in $NEMR_{OA}$. An observed decrease in Δf_{60} with no decrease in OA concentration during the Francis Marion fire may be related to chemical reactions of compounds that fragment to m/z 60 or to differences in the volatility of these compounds compared to the bulk OA. The mechanistic driver of all transformations will be explored below.

The increase in Δf_{44} with plume age for both fires indicates a compositional change toward increasing mass fractional contributions from molecules that fragment to CO_2^+. If only dilution (and hence, evaporation) was occurring in the plumes as they moved downwind, Δf_{44} should be conserved, provided its parent's volatility is similar to that of the bulk of the emitted OA. The observed increase in CO_2^+ in these photochemically-active environments may indicate that production of SOA occurred within the plumes, although there were no statistically-significant increases in the measured downwind $NEMR_{OA}$, as also found in some previous field studies (e.g., Capes et al., 2008; Cubison et al., 2011). On the other hand, this increase could also indicate that the species fragmenting to m/z 44 are relatively less volatile than the bulk OA that evaporates during transport and dilution.

There is experimental evidence investigating chemically-resolved volatility that is consistent with the evaporation of bulk OA resulting in a relative increase in m/z 44 and a

388 relative decrease in *m*/*z* 60. Huffman et al. (2009a) demonstrated for ambient samples in two
389 different megacities that, at a given temperature in a thermodenuder, *m*/*z* 60 evaporated to a
390 greater extent than the bulk OA, while *m*/*z* 44 evaporated to a lesser extent than the bulk OA.
391 While heating OA is technically not the same as diluting OA, the response of OA to increased
392 temperature is analogous to the response of OA to increased dilution. Furthermore, Collier and
393 Zhang (2013) demonstrated that f_{44} increased with decreasing C_{OA} for vehicle test data in the
394 absence of chemistry and hypothesized that this observation was attributable to preferential
395 evaporation of less-oxidized OA species. Thus, the observed changes during SCREAM in Δf_{44}
396 and Δf_{60} may be due, at least in part, to physical changes occurring as some of the emitted OA is
397 volatilized upon dilution with ambient air.

398 Another framework for tracking the chemical evolution of OA was suggested by Heald et
399 al. (2010), who proposed the use of elemental ratios (hydrogen to carbon, H:C, and oxygen to
400 carbon, O:C) to describe photochemical aging of OA. Similar to the fragment evolution, with
401 increasing OH exposure, H:C is expected to decrease (e.g., due to hydrogen abstraction
402 reactions) and O:C is expected to increase (e.g., due to oxygen addition to alkyl radicals). In
403 Figure 5 we present the evolution of the elemental ratio of H:C and O:C during atmospheric
404 transport of the biomass burning plumes from both fires; values of the ratios for the average
405 background, out-of-plume ratio for each fire are shown as dotted lines. We assume uncertainties
406 of 31% of O:C and 10% for H:C, based on Aiken et al. (2008).

407 For both fires, the average background H:C ratio was roughly 15% greater than the H:C
408 at the source; downwind H:C values were mostly within the source variability. As the plumes
409 were transported downwind and mixed with background OA, based on measured dilution rates
410 we expected H:C to have increased toward the background values on a 2- to 3-hour timescale if

411 it were a conserved tracer. The lack of a clear increase with time since emission in both
412 experiments suggests either that loss of both H and C occurred in the plume, or increases in C
413 occurred without corresponding addition of H that would maintain the H:C observed at the
414 source. Typically, H:C decreases with increasing oxidation (Heald et al., 2010).

415 For O:C, about half the downwind values were higher than could be explained by
416 measured variability at the source, and the background OA had O:C within (but at the lower end)
417 of the range at the source. Dilution with background air was thus expected to have had little
418 impact on O:C if O:C were a conserved tracer. Like *m*/*z* 44, O:C could have increased with time
419 if photochemical production and condensation of high O:C species or photochemical aging of
420 aerosol had occurred (Kroll et al., 2011).

421 However, the observed decreases in $NEMR_{OA}$ (whether statistically significant or not)
422 suggests that changes in H:C and O:C may potentially be induced by a solely physical process
423 (i.e., if C were lost from the aerosol phase by preferential evaporation of species that had lower
424 O:C than the average observed at the source). In fact, Huffman et al. (2009b) demonstrated that
425 O:C increased and H:C decreased with increasing evaporation of bulk OA in biomass burning
426 emissions during thermodenuder experiments. Hence, evaporative transformations may be
427 difficult to differentiate from oxidative transformations.

428 ## 3.2. Physical Transformations of Organic Aerosol

429 A net loss of OA due solely to dilution-driven evaporation may thus be consistent with
430 the observations in Figures 2-5. However, we note that we cannot definitively state that no
431 aerosol chemistry has occurred within the plumes as they age. In the following, we assume a
432 priori knowledge that dilution-driven evaporation dominates over chemical processing and
433 explore if the volatility distribution derived by May et al. (2013) for laboratory biomass burning

434 POA can reproduce our airborne observations. If it can, no oxidative chemistry is required to
435 explain the data, although it is possible that some occurs.

436 Simulations representing the process of dilution alone are presented in Figure 6, which
437 shows EF_{OA} data (representing the emission factors near the source and export factors
438 downwind) as a function of the total mass concentration of observed organic aerosol (i.e., not
439 background corrected), C_{OA}, for six flights. Model curves were calculated using the following
440 equation (Donahue et al., 2006; Robinson et al., 2010):

441 $$EF_{OA} = EF_{tot} \sum_i f_i \left(1 + \frac{C_i^*}{C_{OA}}\right)^{-1} \quad (3)$$

442 where *i* represents arbitrarily-chosen surrogate compounds defined by their saturation
443 concentration (C_i*; related to saturation vapor pressure through the ideal gas law), and f_i is the
444 mass fraction of each species *i* relative to the total emitted organics. The set of f_i and C_i* is
445 referred to as a volatility distribution. Here, we utilize the volatility distribution for emissions
446 from open biomass burning that was proposed by May et al. (2013), which is comprised of
447 surrogate compounds representing seven logarithmically-spaced C_i* bins. C_{OA} represents the
448 total OA concentration (emissions + background).

449 EF_{tot} is the emission factor of total organics (gas + particle phase) that are constrained by
450 the volatility distribution (here, all material between $C_i^* = 3x10^{-3}$ μg m^{-3} and $3x10^4$ μg m^{-3}, so
451 this is not equivalent to NMOG), and hence, contribute to gas-particle partitioning; EF_{tot} is likely
452 dominated by biomass-burning-derived organics but may include background semi-volatile
453 organic material that can partition into the particle phase due to the presence of the biomass
454 burning smoke. Values of EF_{tot} were inferred using Equation 3 with measured C_{OA}, calculated
455 EF_{OA} (from Equation 2), and the volatility distribution from May et al. (2013) as inputs for each
456 plume intercept. In Figure 6, the lines represent predictions based on the average EF_{tot} inferred

457 for each fire, while the shaded areas represent ± one standard deviation in EF_{tot}. Values of EF_{tot}
458 ranged from roughly 2 g kg-fuel^{-1} (Bamberg B) to 12 g kg-fuel^{-1} (FJ 22b); both the FJ 9b and
459 Francis Marion fires had inferred EF_{tot} of roughly 6 g kg-fuel^{-1}. Equation 3 implies that EF_{OA}
460 (regardless of whether this represents an emission factor or export factor) decreases with
461 increasing dilution, due to the physical repartitioning of semi-volatile species.

462 There are some key assumptions to our use of Equation 3. We assume that the gas-
463 particle partitioning of the OA can be described using a parameterization derived for laboratory
464 fires, even though the OA in our samples has originated from prescribed fires in the field and
465 may be enhanced by background semi-volatile organics. We are also assuming that EF_{tot} is
466 constant in time for a given prescribed fire (i.e., it does not vary due to source variability, mixing
467 with background air, or atmospheric chemistry). Finally, we are inherently assuming that the
468 plume temperature is constant at 298 K, so dilution is the only process affecting gas-particle
469 partitioning. While these assumptions are not strictly true, they should not affect our conclusions
470 significantly on average.

471 Figures 6a and 6b provide EF_{OA} calculated near the source and downwind for the FJ 9b
472 and Francis Marion fires, respectively. Near-source data from the FJ 22b and Georgetown fires
473 are presented in Figure 6c, and from the Bamberg fires in Figure 6d. Generally, the near-source
474 data for all fires follow the expected trend, exhibiting a decrease in EF_{OA} with decreasing total
475 measured (i.e., not background-corrected) C_{OA}, as would be expected for a semi-volatile tracer
476 with the characteristics summarized by May et al. (2013); variability in near-source data arises
477 due to proximity to the source and to the center of the plume as well as the smoke production
478 rate. Downwind data (only available for Figures 6a and 6b) also generally follow the trend
479 predicted by Equation 3; indeed, downwind OA concentrations appear to be lower than

480 predicted, suggesting evaporation of emitted OA dominates over production and condensation of
481 SOA if occurring. Performing a t-test on the inferred EF_{tot} for both the FJ 9b and Francis Marion
482 fires indicates that the differences between near-source and downwind values are not statistically
483 significant (*p*-value > 0.1), suggesting no observable SOA production from oxidation reactions
484 (e.g., excess OA has reached equilibrium).

485 We also note that the predictions in Figure 6 are based on a composite volatility
486 distribution that best represented biomass fuels investigated in the laboratory during the
487 FLAME-III study, which has been extrapolated to the field in this study. Also, fire behavior was
488 variable during the several hours over which data were collected, as evident in the MCE
489 variability (Akagi et al., 2013); the emissions of organics has been demonstrated to vary with
490 MCE (May et al., 2014; McMeeking et al., 2009). All data are represented using a single set of
491 model inputs, which does not account for this variability with MCE. While other factors likely
492 play a role, these two are likely to be the most important. Regardless, the differences in OA
493 observed at the source and downwind for these plumes can be explained by a simple model of
494 gas-particle partitioning.

495 4. Conclusions

496 In this work, we present field observations of the physicochemical evolution of the
497 organic aerosol present in biomass burning plumes from two prescribed fires in South Carolina.
498 Downwind observations of rBC to CO ratios and emission factors of CO, and CO_2 are not
499 statistically different on average from those at the source. The downwind ratio of OA to CO was
500 significantly lower than at the source for the fire that we were able to follow downwind for up to
501 five hours of atmospheric aging. The downwind OA to CO ratio was not significantly different

502 downwind for the other fire, which may be related to the much shorter observable atmospheric
503 aging time (~2 hr).

504 We observed significant differences in downwind ratios of AMS mass fragments thought
505 to be indicative of fresh biomass burning emissions (*m*/*z* 60, which decreased) and more oxidized
506 OA species (*m*/*z* 44, which increased), consistent with prior reported laboratory photo-oxidation
507 experiments. While the observed increases in Δf_{44} (and the O:C ratio) imply the possibility of
508 SOA production within the plume, these observed changes are also consistent with differences in
509 the volatilities of the species fragmenting to *m/z* 60 and *m/z* 44 relative to the bulk OA, resulting
510 in differences in evaporation as the plume dilutes into background air.

511 Our observations and model simulations suggest that dilution-driven evaporation out of
512 the particle phase dominated over condensation of semi-volatile material into the particle phase
513 over roughly the first two hours of transport during the FJ 9b fire. After this, the OA in the
514 plume reached an apparent steady-state with the background in our observations, as there is no
515 net change to $NEMR_{OA}$ (i.e., there is no obvious dilution-driven evaporation or SOA
516 production); thus, OA transformation can be predicted with a simple gas-particle partitioning
517 model. For the Francis Marion fire, due to limited downwind data, we cannot draw a similar
518 conclusion with any certainty. The decrease in $NEMR_{OA}$ for the FJ 9b fire is consistent with
519 results from previous literature (Akagi et al., 2012; Jolleys et al., 2012, 2015); however, other
520 studies report increases in OA with increasing plume age (DeCarlo et al., 2008; Vakkari et al.,
521 2014; Yokelson et al., 2009). The exact cause of this variability in observations is unclear. These
522 remaining unexplained differences among different field studies highlight the need for additional
523 research on atmospheric physicochemical transformations of biomass burning plumes.

Acknowledgements

We acknowledge funding from the Joint Fire Science Program under project JFSP 11-1-5-12 to S.M.K. and the Strategic Environmental Research and Development Program project RC-1649 administered partly through the Forest Service Research Joint Venture Agreement 08JV11272166039 to R.Y. Additional flight hours and CRDS data were provided by Joint Fire Science Program project 08-1-6-09 to S.U. Adaptation of the Twin Otter was supported by NSF grants ATM-0531044 and ATM-0936321 to R.Y. We also thank Ezra Levin and the NSF/NCAR Research Aviation Facility for assistance with the installation of instruments to the Twin Otter; Shane Murphy, Roya Bahreini, and Ann Middlebrook for guidance in modifying the CSU AMS for aircraft operation; and Jose Jimenez, Tim Onasch, Jill Craven, and Misha Schurman for discussions related to AMS data analysis. This work would not have been possible without the support of the Twin Otter Support Team, especially pilot Bill Mank and mechanic Steve Woods; John Maitland and the forestry staff at Fort Jackson who conducted those prescribed fires; and the Columbia Dispatch Office of the South Carolina Forestry Commission who provided additional prescribed fire locations during the campaign.

5. References

Aiken, A. C., Decarlo, P. F., Kroll, J. H., Worsnop, D. R., Huffman, J. A., Docherty, K. S., Ulbrich, I. M., Mohr, C., Kimmel, J. R., Sueper, D., Sun, Y., Zhang, Q., Trimborn, A., Northway, M., Ziemann, P. J., Canagaratna, M. R., Onasch, T. B., Alfarra, M. R., Prevot, A. S. H., Dommen, J., Duplissy, J., Metzger, A., Baltensperger, U. and Jimenez, J. L.: O/C and OM/OC Ratios of Primary, Secondary, and Ambient Organic Aerosols with High-Resolution Time-of-Flight Aerosol Mass Spectrometry, Environ. Sci. Technol., 42(12), 4478–4485, doi:10.1021/es703009q, 2008.

Akagi, S. K., Burling, I. R., Mendoza, A., Johnson, T. J., Cameron, M., Griffith, D. W. T., Paton-Walsh, C., Weise, D. R., Reardon, J. and Yokelson, R. J.: Field measurements of trace gases emitted by prescribed fires in southeastern US pine forests using an open-path FTIR system, Atmos. Chem. Phys., 14(1), 199–215, doi:10.5194/acp-14-199-2014, 2014.

551 Akagi, S. K., Craven, J. S., Taylor, J. W., McMeeking, G. R., Yokelson, R. J., Burling, I. R.,
552 Urbanski, S. P., Wold, C. E., Seinfeld, J. H., Coe, H., Alvarado, M. J. and Weise, D. R.:
553 Evolution of trace gases and particles emitted by a chaparral fire in California, Atmos. Chem.
554 Phys., 12(3), 1397–1421, doi:10.5194/acp-12-1397-2012, 2012.

555 Akagi, S. K., Yokelson, R. J., Burling, I. R., Meinardi, S., Simpson, I., Blake, D. R.,
556 McMeeking, G. R., Sullivan, A., Lee, T., Kreidenweis, S., Urbanski, S., Reardon, J., Griffith, D.
557 W. T., Johnson, T. J. and Weise, D. R.: Measurements of reactive trace gases and variable O3
558 formation rates in some South Carolina biomass burning plumes, Atmos. Chem. Phys., 13(3),
559 1141–1165, doi:10.5194/acp-13-1141-2013, 2013.

560 Akagi, S. K., Yokelson, R. J., Wiedinmyer, C., Alvarado, M. J., Reid, J. S., Karl, T., Crounse, J.
561 D. and Wennberg, P. O.: Emission factors for open and domestic biomass burning for use in
562 atmospheric models, Atmos. Chem. Phys., 11(9), 4039–4072, doi:10.5194/acp-11-4039-2011,
563 2011.

564 Alfarra, M. R., Prévôt, A. S. H., Szidat, S., Sandradewi, J., Weimer, S., Lanz, V. A., Schreiber,
565 D., Mohr, M. and Baltensperger, U.: Identification of the Mass Spectral Signature of Organic
566 Aerosols from Wood Burning Emissions, Environ. Sci. Technol., 41(16), 5770–5777,
567 doi:10.1021/es062289b, 2007.

568 Allan, J. D., Delia, A. E., Coe, H., Bower, K. N., Alfarra, M. R., Jimenez, J. L., Middlebrook, A.
569 M., Drewnick, F., Onasch, T. B., Canagaratna, M. R., Jayne, J. T. and Worsnop, D. R.: A
570 generalised method for the extraction of chemically resolved mass spectra from Aerodyne
571 aerosol mass spectrometer data, J. Aerosol Sci., 35(7), 909–922,
572 doi:10.1016/j.jaerosci.2004.02.007, 2004.

573 Andreae, M. O. and Gelencsér, A.: Black carbon or brown carbon? The nature of light-absorbing
574 carbonaceous aerosols, Atmos. Chem. Phys., 6(10), 3131–3148, doi:10.5194/acp-6-3131-2006,
575 2006.

576 Andreae, M. O. and Merlet, P.: Emission of trace gases and aerosols from biomass burning,
577 Global Biogeochem. Cycles, 15(4), 955–966, doi:10.1029/2000GB001382, 2001.

578 Bahreini, R., Dunlea, E. J., Matthew, B. M., Simons, C., Docherty, K. S., DeCarlo, P. F.,
579 Jimenez, J. L., Brock, C. A. and Middlebrook, A. M.: Design and Operation of a Pressure-
580 Controlled Inlet for Airborne Sampling with an Aerodynamic Aerosol Lens, Aerosol Sci.
581 Technol., 42(6), 465–471, doi:10.1080/02786820802178514, 2008.

582 Bond, T. C., Doherty, S. J., Fahey, D. W., Forster, P. M., Berntsen, T., DeAngelo, B. J., Flanner,
583 M. G., Ghan, S., Kärcher, B., Koch, D., Kinne, S., Kondo, Y., Quinn, P. K., Sarofim, M. C.,
584 Schultz, M. G., Schulz, M., Venkataraman, C., Zhang, H., Zhang, S., Bellouin, N., Guttikunda,
585 S. K., Hopke, P. K., Jacobson, M. Z., Kaiser, J. W., Klimont, Z., Lohmann, U., Schwarz, J. P.,
586 Shindell, D., Storelvmo, T., Warren, S. G. and Zender, C. S.: Bounding the role of black carbon
587 in the climate system: A scientific assessment, J. Geophys. Res. Atmos., 118(11), 5380–5552,
588 doi:10.1002/jgrd.50171, 2013.

589 Burling, I. R., Yokelson, R. J., Akagi, S. K., Urbanski, S. P., Wold, C. E., Griffith, D. W. T.,
590 Johnson, T. J., Reardon, J. and Weise, D. R.: Airborne and ground-based measurements of the
591 trace gases and particles emitted by prescribed fires in the United States, Atmos. Chem. Phys.,
592 11(23), 12197–12216, doi:10.5194/acp-11-12197-2011, 2011.

593 Burling, I. R., Yokelson, R. J., Griffith, D. W. T., Johnson, T. J., Veres, P., Roberts, J. M.,
594 Warneke, C., Urbanski, S. P., Reardon, J., Weise, D. R., Hao, W. M. and de Gouw, J.:
595 Laboratory measurements of trace gas emissions from biomass burning of fuel types from the
596 southeastern and southwestern United States, Atmos. Chem. Phys., 10(22), 11115–11130,
597 doi:10.5194/acp-10-11115-2010, 2010.

598 Capes, G., Johnson, B., McFiggans, G., Williams, P. I., Haywood, J. and Coe, H.: Aging of
599 biomass burning aerosols over West Africa: Aircraft measurements of chemical composition,
600 microphysical properties, and emission ratios, J. Geophys. Res., 113, D00C15,
601 doi:10.1029/2008JD009845, 2008.

602 Christian, T. J., Kleiss, B., Yokelson, R. J., Holzinger, R., Crutzen, P. J., Hao, W. M., Saharjo, B.
603 H. and Ward, D. E.: Comprehensive laboratory measurements of biomass-burning emissions: 1.
604 Emissions from Indonesian, African, and other fuels, J. Geophys. Res., 108(D23), 4719,
605 doi:10.1029/2003JD003704, 2003.

606 Collier, S. and Zhang, Q.: Gas-phase CO2 subtraction for improved measurements of the organic
607 aerosol mass concentration and oxidation degree by an aerosol mass spectrometer., Environ. Sci.
608 Technol., 47(24), 14324–31, doi:10.1021/es404024h, 2013.

609 Cubison, M. J., Ortega, A. M., Hayes, P. L., Farmer, D. K., Day, D., Lechner, M. J., Brune, W.
610 H., Apel, E., Diskin, G. S., Fisher, J. A., Fuelberg, H. E., Hecobian, A., Knapp, D. J., Mikoviny,
611 T., Riemer, D., Sachse, G. W., Sessions, W., Weber, R. J., Weinheimer, A. J., Wisthaler, A. and
612 Jimenez, J. L.: Effects of aging on organic aerosol from open biomass burning smoke in aircraft
613 and laboratory studies, Atmos. Chem. Phys., 11(23), 12049–12064, doi:10.5194/acp-11-12049-
614 2011, 2011.

615 DeCarlo, P. F., Dunlea, E. J., Kimmel, J. R., Aiken, A. C., Sueper, D., Crounse, J., Wennberg, P.
616 O., Emmons, L., Shinozuka, Y., Clarke, A., Zhou, J., Tomlinson, J., Collins, D. R., Knapp, D.,
617 Weinheimer, A. J., Montzka, D. D., Campos, T. and Jimenez, J. L.: Fast airborne aerosol size
618 and chemistry measurements above Mexico City and Central Mexico during the MILAGRO
619 campaign, Atmos. Chem. Phys., 8(14), 4027–4048, doi:10.5194/acp-8-4027-2008, 2008.

620 DeCarlo, P. F., Kimmel, J. R., Trimborn, A., Northway, M. J., Jayne, J. T., Aiken, A. C., Gonin,
621 M., Fuhrer, K., Horvath, T., Docherty, K. S., Worsnop, D. R. and Jimenez, J. L.: Field-
622 deployable, high-resolution, time-of-flight aerosol mass spectrometer., Anal. Chem., 78(24),
623 8281–9, doi:10.1021/ac061249n, 2006.

624 Donahue, N. M., Chuang, W., Epstein, S. A., Kroll, J. H., Worsnop, D. R., Robinson, A. L.,
625 Adams, P. J. and Pandis, S. N.: Why do organic aerosols exist? Understanding aerosol lifetimes

using the two-dimensional volatility basis set, Environ. Chem., 10(3), 151, doi:10.1071/EN13022, 2013.

Heald, C. L., Kroll, J. H., Jimenez, J. L., Docherty, K. S., DeCarlo, P. F., Aiken, A. C., Chen, Q., Martin, S. T., Farmer, D. K. and Artaxo, P.: A simplified description of the evolution of organic aerosol composition in the atmosphere, Geophys. Res. Lett., 37(8), L08803, doi:10.1029/2010GL042737, 2010.

Heilman, W. E., Liu, Y., Urbanski, S., Kovalev, V. and Mickler, R.: Wildland fire emissions, carbon, and climate: Plume rise, atmospheric transport, and chemistry processes, For. Ecol. Manage., 317, 70–79, doi:10.1016/j.foreco.2013.02.001, 2014.

Hennigan, C. J., Miracolo, M. A., Engelhart, G. J., May, A. A., Presto, A. A., Lee, T., Sullivan, A. P., McMeeking, G. R., Coe, H., Wold, C. E., Hao, W.-M., Gilman, J. B., Kuster, W. C., de Gouw, J., Schichtel, B. A., Kreidenweis, S. M. and Robinson, A. L.: Chemical and physical transformations of organic aerosol from the photo-oxidation of open biomass burning emissions in an environmental chamber, Atmos. Chem. Phys., 11(15), 7669–7686, doi:10.5194/acp-11-7669-2011, 2011.

Hennigan, C. J., Sullivan, A. P., Collett, J. L. and Robinson, A. L.: Levoglucosan stability in biomass burning particles exposed to hydroxyl radicals, Geophys. Res. Lett., 37(9), n/a–n/a, doi:10.1029/2010GL043088, 2010.

Hobbs, P. V., Sinha, P., Yokelson, R. J., Christian, T. J., Blake, D. R., Gao, S., Kirchstetter, T. W., Novakov, T. and Pilewskie, P.: Evolution of gases and particles from a savanna fire in South Africa, J. Geophys. Res., 108(D13), 8485, doi:10.1029/2002JD002352, 2003.

Hosseini, S., Urbanski, S. P., Dixit, P., Qi, L., Burling, I. R., Yokelson, R. J., Johnson, T. J., Shrivastava, M., Jung, H. S., Weise, D. R., Miller, J. W. and Cocker, D. R.: Laboratory characterization of PM emissions from combustion of wildland biomass fuels, J. Geophys. Res. Atmos., 118(17), 9914–9929, doi:10.1002/jgrd.50481, 2013.

Huffman, J. A., Docherty, K. S., Aiken, A. C., Cubison, M. J., Ulbrich, I. M., DeCarlo, P. F., Sueper, D., Jayne, J. T., Worsnop, D. R., Ziemann, P. J. and Jimenez, J. L.: Chemically-resolved aerosol volatility measurements from two megacity field studies, Atmos. Chem. Phys., 9(18), 7161–7182, doi:10.5194/acp-9-7161-2009, 2009a.

Huffman, J. A., Docherty, K. S., Mohr, C., Cubison, M. J., Ulbrich, I. M., Ziemann, P. J., Onasch, T. B. and Jimenez, J. L.: Chemically-Resolved Volatility Measurements of Organic Aerosol from Different Sources, Environ. Sci. Technol., 43(14), 5351–5357, doi:10.1021/es803539d, 2009b.

Jolleys, M. D., Coe, H., McFiggans, G., Capes, G., Allan, J. D., Crosier, J., Williams, P. I., Allen, G., Bower, K. N., Jimenez, J. L., Russell, L. M., Grutter, M. and Baumgardner, D.: Characterizing the aging of biomass burning organic aerosol by use of mixing ratios: a meta-

662 analysis of four regions., Environ. Sci. Technol., 46(24), 13093–102, doi:10.1021/es302386v,
663 2012.

664 Jolleys, M. D., Coe, H., McFiggans, G., McMeeking, G. R., Lee, T., Kreidenweis, S. M., Collett,
665 J. L. and Sullivan, A. P.: Organic aerosol emission ratios from the laboratory combustion of
666 biomass fuels, J. Geophys. Res. Atmos., 119(22), 12,850–12,871, doi:10.1002/2014JD021589,
667 2014.

668 Jolleys, M. D., Coe, H., Mcfiggans, G., Taylor, J. W., Shea, S. J. O., Breton, M. Le, Bauguitte, S.
669 J., Moller, S., Carlo, P. Di, Aruffo, E., Palmer, P. I., Lee, J. D., Percival, C. J. and Gallagher, M.
670 W.: Properties and evolution of biomass burning organic aerosol from Canadian boreal forest
671 fires, Atmos. Chem. Phys., 15(6), 3077–3095, doi:10.5194/acp-15-3077-2015, 2015.

672 Kirchstetter, T. W., Novakov, T. and Hobbs, P. V.: Evidence that the spectral dependence of
673 light absorption by aerosols is affected by organic carbon, J. Geophys. Res., 109(D21), D21208,
674 doi:10.1029/2004JD004999, 2004.

675 Kroll, J. H., Donahue, N. M., Jimenez, J. L., Kessler, S. H., Canagaratna, M. R., Wilson, K. R.,
676 Altieri, K. E., Mazzoleni, L. R., Wozniak, A. S., Bluhm, H., Mysak, E. R., Smith, J. D., Kolb, C.
677 E. and Worsnop, D. R.: Carbon oxidation state as a metric for describing the chemistry of
678 atmospheric organic aerosol., Nat. Chem., 3(2), 133–9, doi:10.1038/nchem.948, 2011.

679 Lack, D. A., Langridge, J. M., Bahreini, R., Cappa, C. D., Middlebrook, A. M. and Schwarz, J.
680 P.: Brown carbon and internal mixing in biomass burning particles., Proc. Natl. Acad. Sci. U. S.
681 A., 109(37), 14802–7, doi:10.1073/pnas.1206575109, 2012.

682 Lee, T., Sullivan, A. P., Mack, L., Jimenez, J. L., Kreidenweis, S. M., Onasch, T. B., Worsnop,
683 D. R., Malm, W., Wold, C. E., Hao, W. M. and Collett, J. L.: Chemical Smoke Marker
684 Emissions During Flaming and Smoldering Phases of Laboratory Open Burning of Wildland
685 Fuels, Aerosol Sci. Technol., 44(9), i–v, doi:10.1080/02786826.2010.499884, 2010.

686 Marple, V. A., Rubow, K. L. and Behm, S. M.: A Microorifice Uniform Deposit Impactor
687 (MOUDI): Description, Calibration, and Use, Aerosol Sci. Technol., 14(4), 434–446,
688 doi:10.1080/02786829108959504, 1991.

689 May, A. A., Levin, E. J. T., Hennigan, C. J., Riipinen, I., Lee, T., Collett, J. L., Jimenez, J. L.,
690 Kreidenweis, S. M. and Robinson, A. L.: Gas-particle partitioning of primary organic aerosol
691 emissions: 3. Biomass burning, J. Geophys. Res. Atmos., 118(19), 11,327–11,338,
692 doi:10.1002/jgrd.50828, 2013.

693 May, A. A., McMeeking, G. R., Lee, T., Taylor, J. W., Craven, J. S., Burling, I., Sullivan, A. P.,
694 Akagi, S., Collett, J. L., Flynn, M., Coe, H., Urbanski, S. P., Seinfeld, J. H., Yokelson, R. J. and
695 Kreidenweis, S. M.: Aerosol emissions from prescribed fires in the United States: A synthesis of
696 laboratory and aircraft measurements, J. Geophys. Res. Atmos., 119(20), 11,826–11,849,
697 doi:10.1002/2014JD021848, 2014.

May, A. A., Saleh, R., Hennigan, C. J., Donahue, N. M. and Robinson, A. L.: Volatility of organic molecular markers used for source apportionment analysis: measurements and implications for atmospheric lifetime., Environ. Sci. Technol., 46(22), 12435–44, doi:10.1021/es302276t, 2012.

McMeeking, G. R., Kreidenweis, S. M., Baker, S., Carrico, C. M., Chow, J. C., Collett, J. L., Hao, W. M., Holden, A. S., Kirchstetter, T. W., Malm, W. C., Moosmüller, H., Sullivan, A. P. and Wold, C. E.: Emissions of trace gases and aerosols during the open combustion of biomass in the laboratory, J. Geophys. Res., 114(D19), D19210, doi:10.1029/2009JD011836, 2009.

Middlebrook, A. M., Bahreini, R., Jimenez, J. L. and Canagaratna, M. R.: Evaluation of Composition-Dependent Collection Efficiencies for the Aerodyne Aerosol Mass Spectrometer using Field Data, Aerosol Sci. Technol., 46(3), 258–271, doi:10.1080/02786826.2011.620041, 2012.

Morgan, W. T., Allan, J. D., Bower, K. N., Highwood, E. J., Liu, D., McMeeking, G. R., Northway, M. J., Williams, P. I., Krejci, R. and Coe, H.: Airborne measurements of the spatial distribution of aerosol chemical composition across Europe and evolution of the organic fraction, Atmos. Chem. Phys., 10(8), 4065–4083, doi:10.5194/acp-10-4065-2010, 2010.

Ng, N. L., Canagaratna, M. R., Zhang, Q., Jimenez, J. L., Tian, J., Ulbrich, I. M., Kroll, J. H., Docherty, K. S., Chhabra, P. S., Bahreini, R., Murphy, S. M., Seinfeld, J. H., Hildebrandt, L., Donahue, N. M., DeCarlo, P. F., Lanz, V. A., Prévôt, A. S. H., Dinar, E., Rudich, Y. and Worsnop, D. R.: Organic aerosol components observed in Northern Hemispheric datasets from Aerosol Mass Spectrometry, Atmos. Chem. Phys., 10(10), 4625–4641, doi:10.5194/acp-10-4625-2010, 2010.

Ortega, A. M., Day, D. A., Cubison, M. J., Brune, W. H., Bon, D., de Gouw, J. A. and Jimenez, J. L.: Secondary organic aerosol formation and primary organic aerosol oxidation from biomass-burning smoke in a flow reactor during FLAME-3, Atmos. Chem. Phys., 13(22), 11551–11571, doi:10.5194/acp-13-11551-2013, 2013.

Reid, J. S., Koppmann, R., Eck, T. F. and Eleuterio, D. P.: A review of biomass burning emissions part II: intensive physical properties of biomass burning particles, Atmos. Chem. Phys., 5(3), 799–825, doi:10.5194/acp-5-799-2005, 2005.

Robinson, A. L., Grieshop, A. P., Donahue, N. M. and Hunt, S. W.: Updating the Conceptual Model for Fine Particle Mass Emissions from Combustion Systems, J. Air Waste Manage. Assoc., 60(10), 1204–1222, doi:10.3155/1047-3289.60.10.1204, 2010.

Schwarz, J. P., Gao, R. S., Fahey, D. W., Thomson, D. S., Watts, L. A., Wilson, J. C., Reeves, J. M., Darbeheshti, M., Baumgardner, D. G., Kok, G. L., Chung, S. H., Schulz, M., Hendricks, J., Lauer, A., Kärcher, B., Slowik, J. G., Rosenlof, K. H., Thompson, T. L., Langford, A. O., Loewenstein, M. and Aikin, K. C.: Single-particle measurements of midlatitude black carbon and light-scattering aerosols from the boundary layer to the lower stratosphere, J. Geophys. Res. Atmos., 111(16), D16207, doi:10.1029/2006JD007076, 2006.

736 Simoneit, B. R. T., Schauer, J. J., Nolte, C. G., Oros, D. R., Elias, V. O., Fraser, M. P., Rogge,
737 W. F. and Cass, G. R.: Levoglucosan, a tracer for cellulose in biomass burning and atmospheric
738 particles, Atmos. Environ., 33(2), 173–182, doi:10.1016/S1352-2310(98)00145-9, 1999.

739 Stephens, M., Turner, N. and Sandberg, J.: Particle Identification by Laser-Induced
740 Incandescence in a Solid-State Laser Cavity, Appl. Opt., 42(19), 3726,
741 doi:10.1364/AO.42.003726, 2003.

742 Sueper, D., DeCarlo, P. F., Aiken, A. C. and Jimenez, J. L.: ToF-AMS High Resolution Analysis
743 Software, [online] Available from: http://cires.colorado.edu/jimenez-group/wiki/index.php/ToF-
744 AMS_Analysis_Software, 2013.

745 Sullivan, A. P., Holden, A. S., Patterson, L. A., McMeeking, G. R., Kreidenweis, S. M., Malm,
746 W. C., Hao, W. M., Wold, C. E. and Collett, J. L.: A method for smoke marker measurements
747 and its potential application for determining the contribution of biomass burning from wildfires
748 and prescribed fires to ambient PM 2.5 organic carbon, J. Geophys. Res., 113(D22), D22302,
749 doi:10.1029/2008JD010216, 2008.

750 Sullivan, A. P., May, A. A., Lee, T., McMeeking, G. R., Kreidenweis, S. M., Akagi, S. K.,
751 Yokelson, R. J., Urbanski, S. P. and Collett Jr., J. L.: Airborne characterization of smoke marker
752 ratios from prescribed burning, Atmos. Chem. Phys., 14(19), 10535–10545, doi:10.5194/acp-14-
753 10535-2014, 2014.

754 Urbanski, S. P.: Combustion efficiency and emission factors for wildfire-season fires in mixed
755 conifer forests of the northern Rocky Mountains, US, Atmos. Chem. Phys., 13(14), 7241–7262,
756 doi:10.5194/acp-13-7241-2013, 2013.

757 Urbanski, S. P., Hao, W. M. and Nordgren, B.: The wildland fire emission inventory: western
758 United States emission estimates and an evaluation of uncertainty, Atmos. Chem. Phys., 11(24),
759 12973–13000, doi:10.5194/acp-11-12973-2011, 2011.

760 Vakkari, V., Kerminen, V.-M., Beukes, J. P., Tiitta, P., van Zyl, P. G., Josipovic, M., Venter, A.
761 D., Jaars, K., Worsnop, D. R., Kulmala, M. and Laakso, L.: Rapid changes in biomass burning
762 aerosols by atmospheric oxidation, Geophys. Res. Lett., 41(7), 2644–2651,
763 doi:10.1002/2014GL059396, 2014.

764 Ward, D. E. and Radke, L. F.: Emissions measurements from vegetation fires: A comparative
765 evaluation of methods and results, in Fire in the Environment: The Ecological, Atmospheric, and
766 Climatic Importance of Vegetation Fires, edited by P. J. Crutzen and J. G. Goldammer, pp. 53–
767 76, John Wiley & Sons, Inc., Chischester, England., 1993.

768 Watson, J. G., Chow, J. C., Chen, L.-W. A., Lowenthal, D. H., Fujita, E. M., Kuhns, H. D.,
769 Sodeman, D. A., Campbell, D. E., Moosmüller, H., Zhu, D. and Motallebi, N.: Particulate
770 emission factors for mobile fossil fuel and biomass combustion sources., Sci. Total Environ.,
771 409(12), 2384–96, doi:10.1016/j.scitotenv.2011.02.041, 2011.

772 Van der Werf, G. R., Randerson, J. T., Giglio, L., Collatz, G. J., Mu, M., Kasibhatla, P. S.,
773 Morton, D. C., DeFries, R. S., Jin, Y. and van Leeuwen, T. T.: Global fire emissions and the
774 contribution of deforestation, savanna, forest, agricultural, and peat fires (1997–2009), Atmos.
775 Chem. Phys., 10(23), 11707–11735, doi:10.5194/acp-10-11707-2010, 2010.

776 Wiedinmyer, C., Akagi, S. K., Yokelson, R. J., Emmons, L. K., Al-Saadi, J. A., Orlando, J. J.
777 and Soja, A. J.: The Fire INventory from NCAR (FINN): a high resolution global model to
778 estimate the emissions from open burning, Geosci. Model Dev., 4(3), 625–641,
779 doi:10.5194/gmd-4-625-2011, 2011.

780 Wiedinmyer, C., Quayle, B., Geron, C., Belote, A., McKenzie, D., Zhang, X., O'Neill, S. and
781 Wynne, K. K.: Estimating emissions from fires in North America for air quality modeling,
782 Atmos. Environ., 40(19), 3419–3432, doi:10.1016/j.atmosenv.2006.02.010, 2006.

783 Wilson, J. C., Lafleu, B. G., Hilbert, H., Seebaugh, W. R., Fox, J., Gesler, D. W., Brock, C. A.,
784 Huebert, B. J. and Mullen, J.: Function and Performance of a Low Turbulence Inlet for Sampling
785 Supermicron Particles from Aircraft Platforms, Aerosol Sci. Technol., 38(8), 790–802,
786 doi:10.1080/027868290500841, 2004.

787 Yokelson, R. J., Burling, I. R., Gilman, J. B., Warneke, C., Stockwell, C. E., de Gouw, J., Akagi,
788 S. K., Urbanski, S. P., Veres, P., Roberts, J. M., Kuster, W. C., Reardon, J., Griffith, D. W. T.,
789 Johnson, T. J., Hosseini, S., Miller, J. W., Cocker III, D. R., Jung, H. and Weise, D. R.: Coupling
790 field and laboratory measurements to estimate the emission factors of identified and unidentified
791 trace gases for prescribed fires, Atmos. Chem. Phys., 13(1), 89–116, doi:10.5194/acp-13-89-
792 2013, 2013a.

793 Yokelson, R. J., Burling, I. R., Gilman, J. B., Warneke, C., Stockwell, C. E., de Gouw, J., Akagi,
794 S. K., Urbanski, S. P., Veres, P., Roberts, J. M., Kuster, W. C., Reardon, J., Griffith, D. W. T.,
795 Johnson, T. J., Hosseini, S., Miller, J. W., Cocker III, D. R., Jung, H. and Weise, D. R.: Coupling
796 field and laboratory measurements to estimate the emission factors of identified and unidentified
797 trace gases for prescribed fires, Atmos. Chem. Phys., 13(1), 89–116, doi:10.5194/acp-13-89-
798 2013, 2013b.

799 Yokelson, R. J., Crounse, J. D., DeCarlo, P. F., Karl, T., Urbanski, S., Atlas, E., Campos, T.,
800 Shinozuka, Y., Kapustin, V., Clarke, A. D., Weinheimer, A., Knapp, D. J., Montzka, D. D.,
801 Holloway, J., Weibring, P., Flocke, F., Zheng, W., Toohey, D., Wennberg, P. O., Wiedinmyer,
802 C., Mauldin, L., Fried, A., Richter, D., Walega, J., Jimenez, J. L., Adachi, K., Buseck, P. R.,
803 Hall, S. R. and Shetter, R.: Emissions from biomass burning in the Yucatan, Atmos. Chem.
804 Phys., 9(15), 5785–5812, doi:10.5194/acp-9-5785-2009, 2009.

805

806

807 # Figures

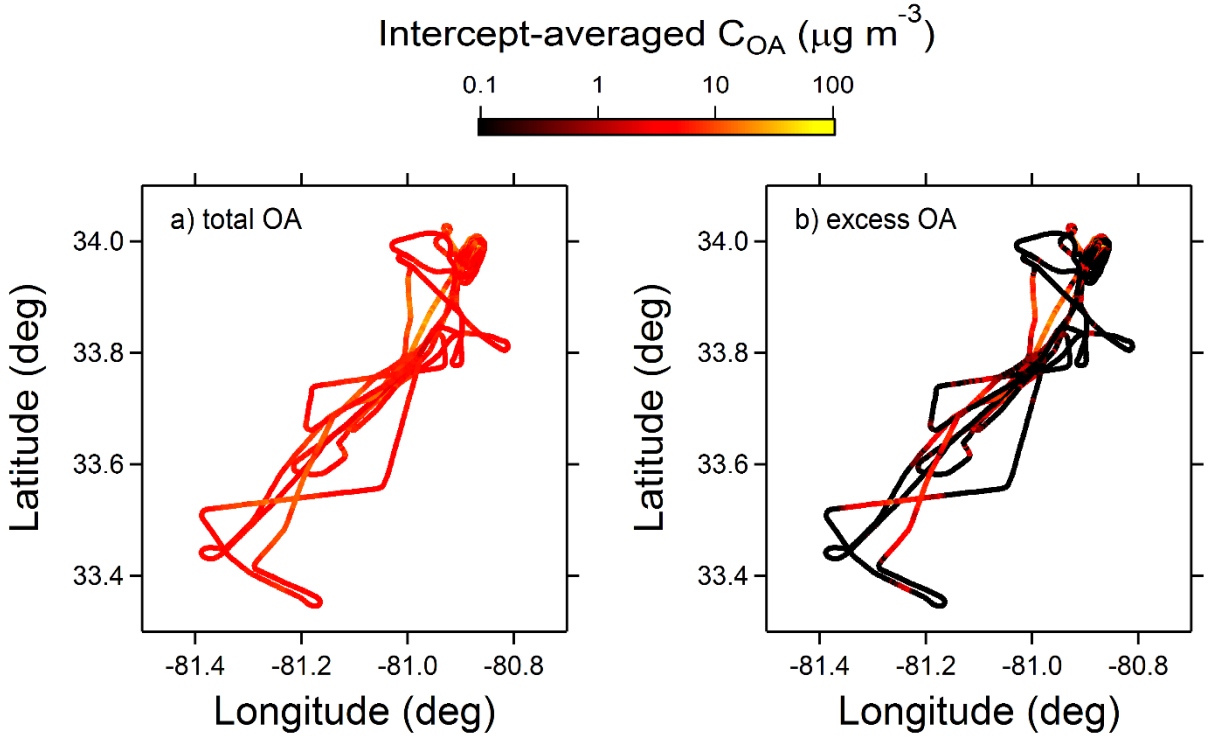

808

809 Figure 1.

810 Flight tracks colored by **a)** total OA concentration and **b)** excess OA concentration. Due to the
811 log-scaling of intercept-averaged concentrations, the minimum value in panel b) is set to 0.1 μg
812 m^{-3}. Removing the background OA elucidates distinct plume transport to the southwest.

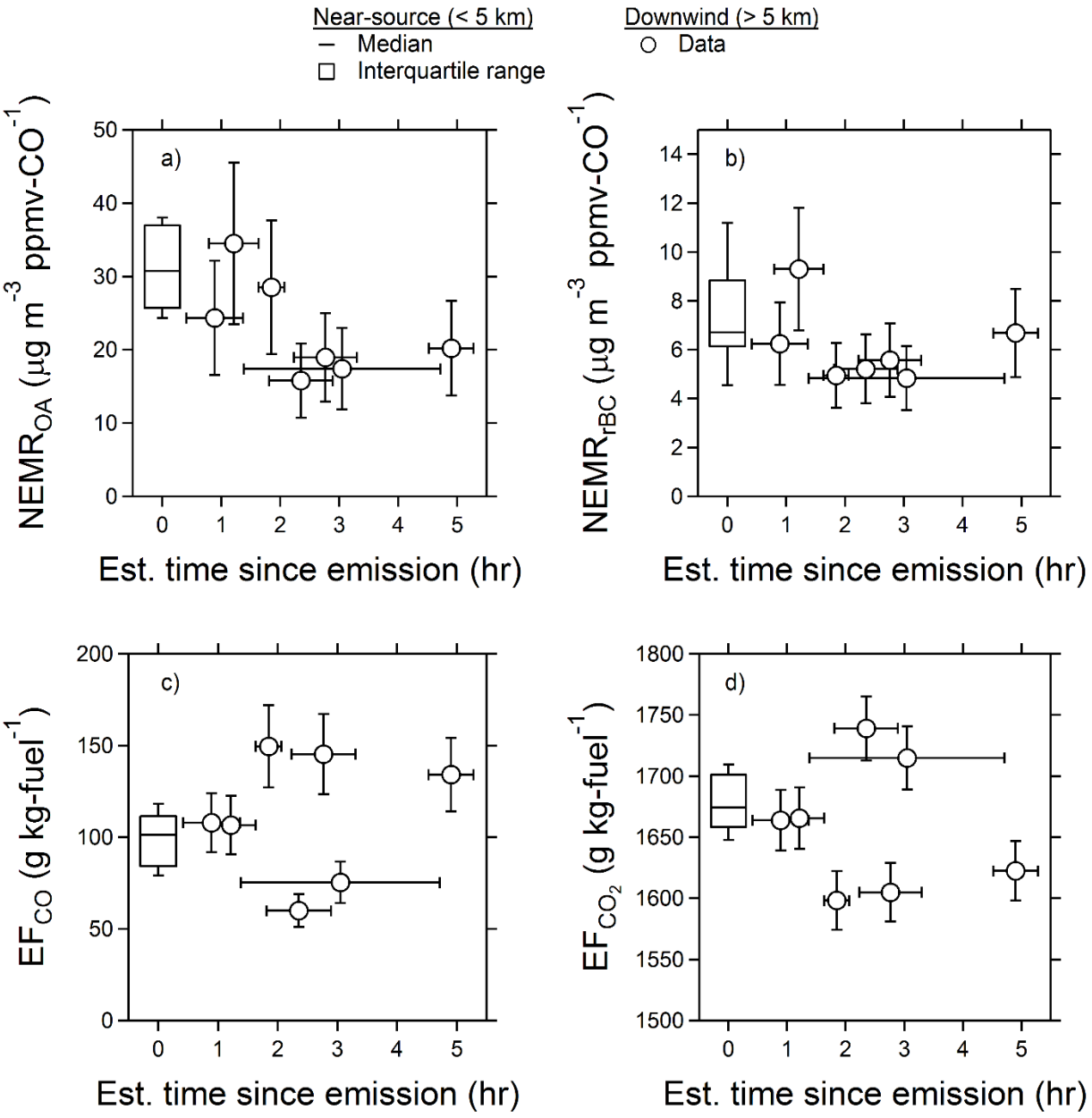

Figure 2.

Near-source and downwind data collected during the FJ 9b prescribed fire. **a)** the ratio of excess OA to CO; **b)** the ratio of excess rBC to CO; **c)** emission/export factor for CO; and **d)** emission/export factor of CO_2. Near-source data are represented by box-and-whisker plots (boxes: 25th and 75th percentiles; whiskers: 10th and 90th percentiles; horizontal lines: median) while downwind data are represented by markers. Error bars associated with the markers indicate range of estimated time since emission (x-direction) and measurement uncertainty (y-direction). Error bars in x direction do not account for estimated 30% accuracy of wind speed.

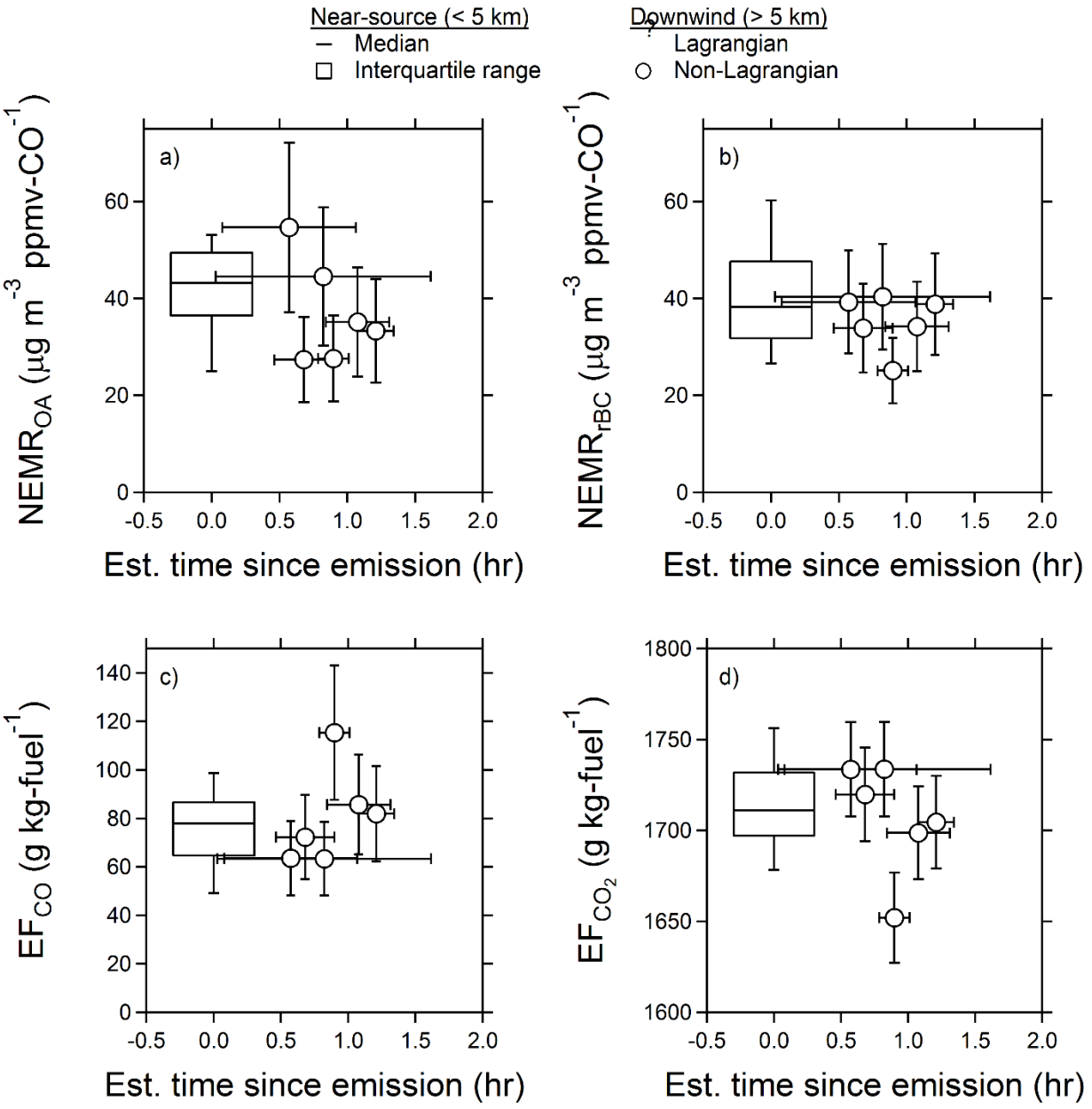

825

826 Figure 3.

827 As in Figure 2, but for the Francis Marion prescribed fire.

828

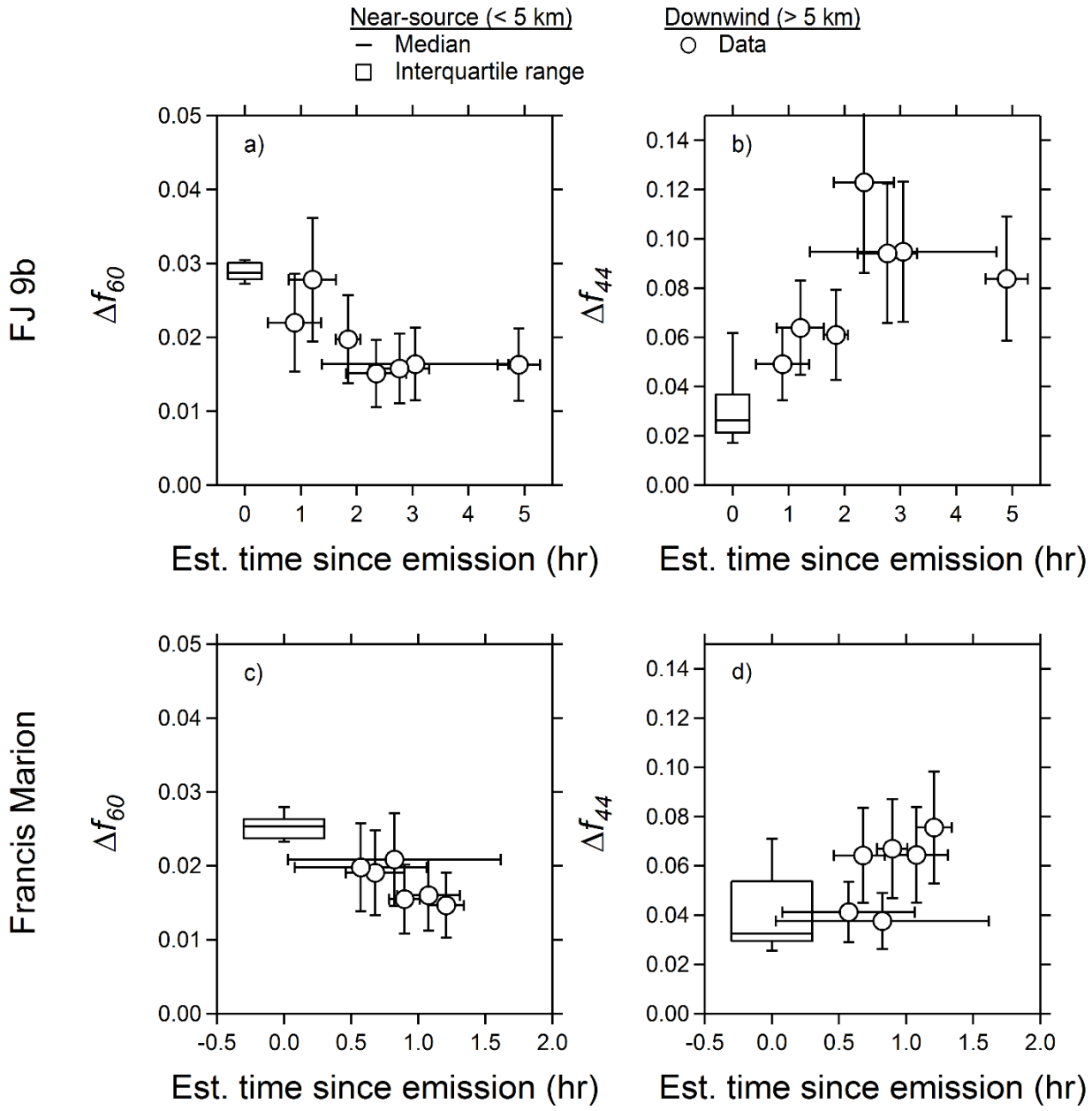

Figure 4.

Evolution of background-corrected AMS mass fractions. **a)** Δf_{60} for the FJ 9b fire; **b)** Δf_{44} for the FJ 9b fire; **c)** Δf_{60} for the Francis Marion fire; **d)** Δf_{44} for the Francis Marion fire. In all panels, there is a statistically-significant difference between data collected near the source and downwind. Box-and-whisker plots and markers are identical to those in Figures 2 and 3.

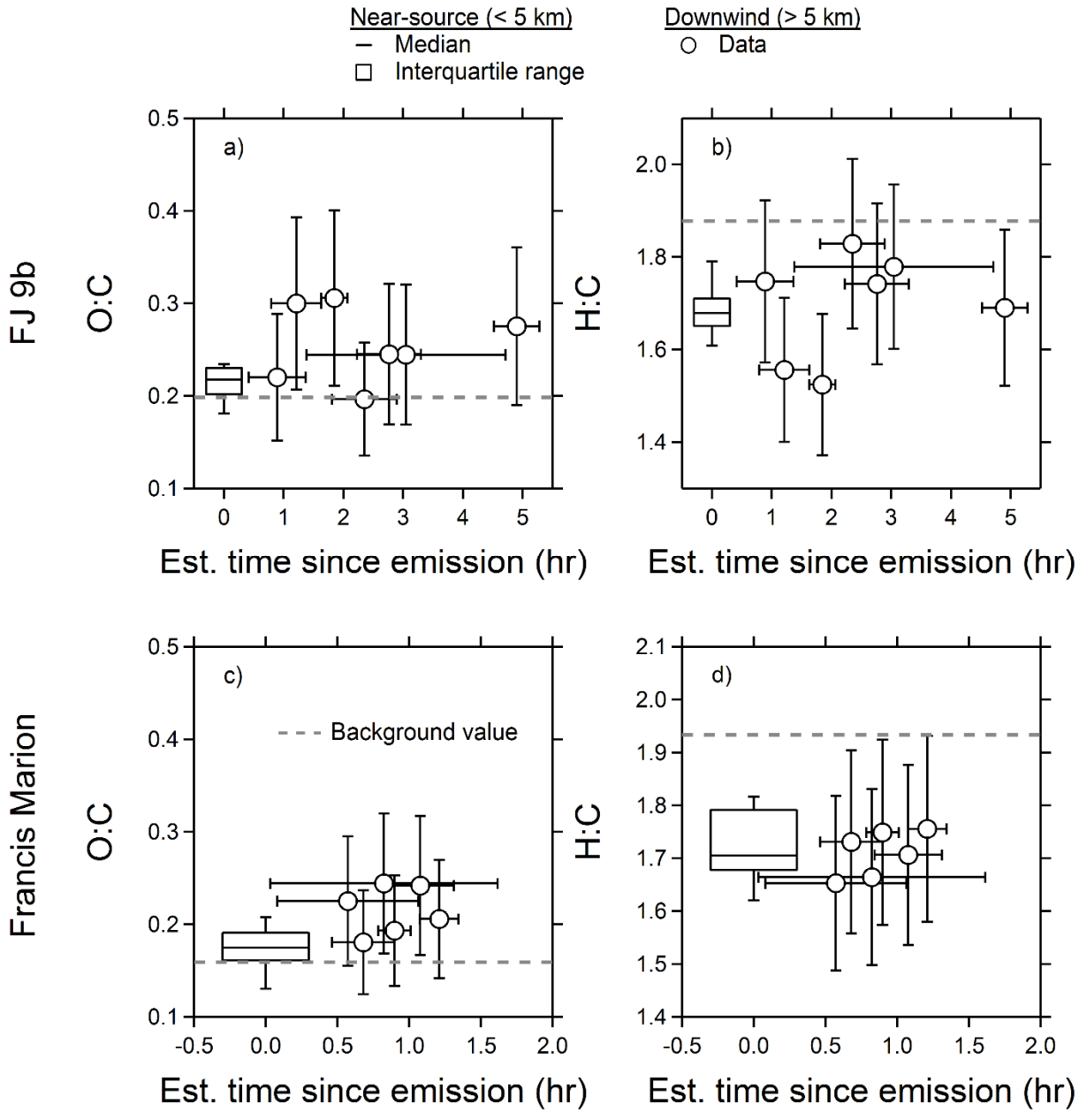

Figure 5.

Evolution of elemental ratios derived from AMS data. **a)** O:C for the FJ 9b fire; **b)** H:C for the FJ 9b fire; **c)** O:C for the Francis Marion fire; **d)** H:C for the Francis Marion fire. For both fires, changes in O:C with increasing estimated time since emission are statistically significant. Dashed line is the value of the parameter in the background measurements outside of plume penetrations. Box-and-whisker plots and markers are identical to those in Figures 2 and 3.

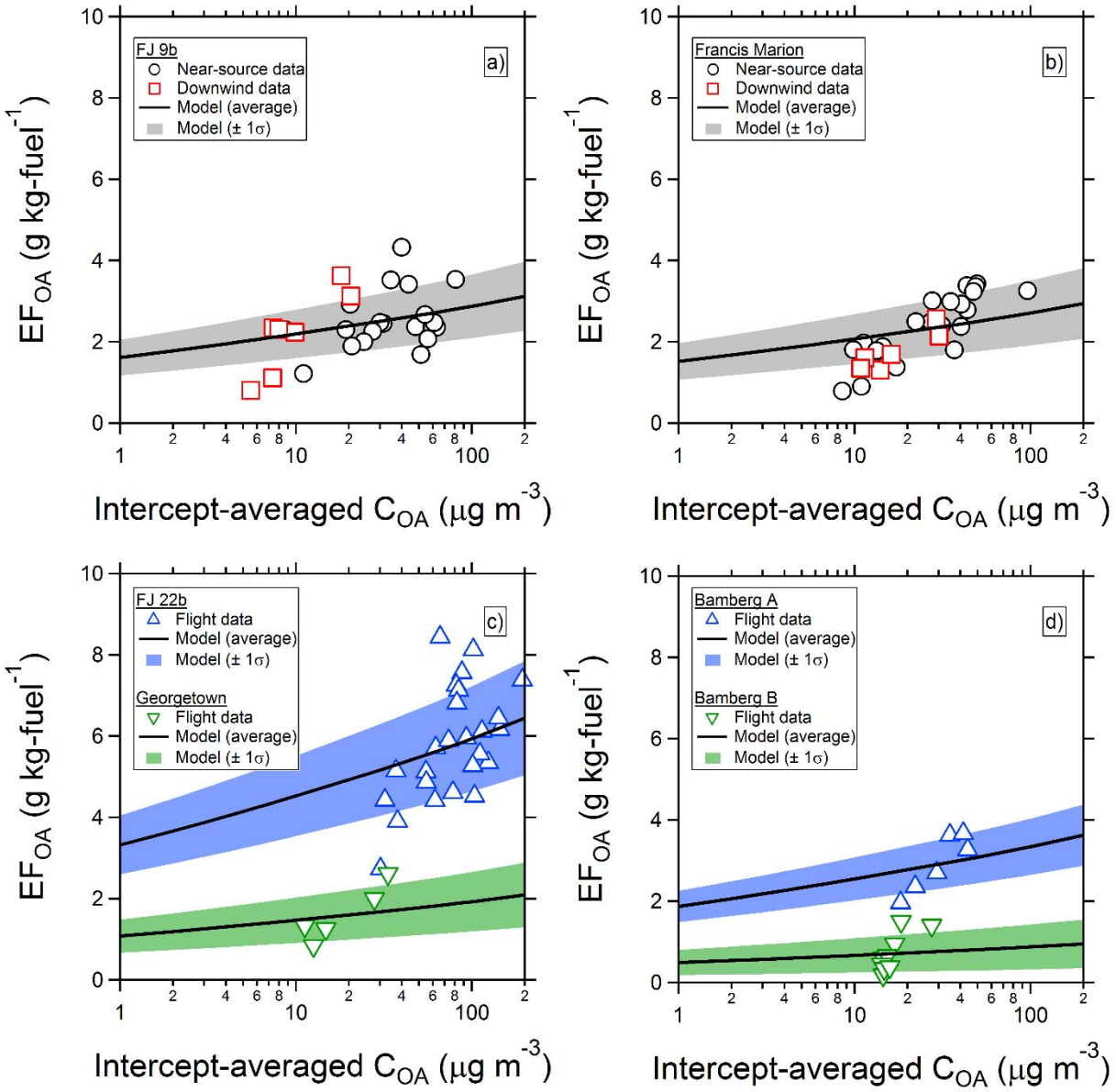

Figure 6.

Changes in the emission factor of excess OA due to gas-particle partitioning as a function of total observed OA. **a)** near-source (circles) and downwind (squares) data for the FJ 9b fire; **b)** near-source (circles) and downwind (squares) data for the Francis Marion fire; **c)** near-source data for the FJ 22b (upward-facing triangles) and Georgetown (downward-facing triangles) fires; and **d)** near-source data for the two fires attributed to the Bamberg site ("A": upward-facing triangles; "B": downward-facing triangles). Curves represent predictions using the laboratory parameterization from May et al. (2013).